Enhanced Local-Area DGNSS for Autonomous Vehicle Navigation: Optimal Smoothing Strategy

Gihun Nam, Dongwoo Kim, Noah Minchan Kim, and Jiyun Lee, *Korea Advanced Institute of Science and Technology (KAIST)*
Sam Pullen, *Stanford University*

ABSTRACT

Local Area Differential GNSS (LADGNSS) is one means of providing navigation and guidance to autonomous vehicles with very high accuracy and integrity. In previous work, the authors have developed a low-cost, portable LADGNSS system prototype based on the single-frequency (L1-only) Ground-based Augmentation System (GBAS) architecture developed for civil aviation. This work expands that system to use multiple frequencies (L5/E5 in addition to L1) and Galileo satellites in addition to GPS, creating a Dual-Frequency Dual-Constellation (DFDC) system. This creates additional options for the carrier smoothing of code phase that is critical to reducing code-phase (pseudorange) errors and provides additional means to detect and exclude signals affected by anomalous ionospheric behavior.

This paper develops new models of nominal errors for DFDC LADGNSS to represent error correlation across time and among ground reference receivers. These models support detailed comparisons of different smoothing algorithms and time constants in the presence of multiple nominal error sources. Vertical Protection Levels (VPLs) for a set of candidate smoothing processes and time constants are generated for 27-satellite GPS and Galileo constellations to determine which give the best performance (lowest VPLs, and thus highest availability) under different operational scenarios, different user distances from the LADGNSS reference station, and different levels of nominal ionospheric activity (in mid-latitudes and in equatorial regions).

1.0 INTRODUCTION

Current and future autonomous vehicles navigate using GNSS along with onboard sensors such as cameras and inertial measurement units (IMUs). The authors' previous work on unmanned aerial vehicle (UAV) navigation (see [10, 13]) has emphasized the use of local-area differential GNSS (LADGNSS) corrections to provide the best possible accuracy and integrity to UAVs within 25 km of a LADGNSS reference station. In [13] and earlier papers, we proposed a design for a LADGNSS reference system based on a simplification of the Ground Based Augmentation System (GBAS) architecture [3] in order to gain the integrity-monitor capabilities of GBAS with a smaller, more portable, and less-expensive system. A variation of this design has been implemented and tested in the flight tests reported in [13].

In the LADGNSS reference system (LRS) described in [10, 13], the basic design of GBAS is retained but simplified, with three reference receivers using commercial survey-grade antennas being sited within 10 – 50 meters of each other. Ground system monitoring is limited to the essentials of measurement quality monitoring (MQM) of the raw and smoothed L1 C/A code and carrier-phase measurements and verification of the navigation data accuracy, signal strength, and measurement consistency across reference receivers. A two-way datalink between the LRS and UAVs allows each UAV to send its protection levels and any airborne monitor alerts back to the LRS as well as to receive corrections and integrity information (along with guidance commands) from it.

This paper modernizes and expands upon our previous work by making use of measurements on the GPS L5 frequency and the Galileo E1 and E5a frequencies, creating a Dual-Frequency, Dual-Constellation (DFDC) version of LADGNSS. This adds many more measurements to GPS L1-only LADGNSS and adds robustness against ionospheric disturbances due to the ability to combine L1/E1 and L5/E5a measurements to remove all or part of the residual (uncorrected) ionospheric errors affecting users. Since several different methods of combining these measurements exist, an analysis is needed to identify the best-performing methods as a function of the operational conditions that DFDC LADGNSS will support and the errors (both nominal and anomalous) that it will encounter.

Section 2.0 provides an introduction to the role of smoothing in LADGNSS and the considerations that apply to the choice of smoothing techniques and time constants. Section 3.0 develops new error models that represent nominal ground and airborne

conditions in the presence of time-correlated multipath errors and ground multipath errors correlated among reference stations. Section 4.0 applies these models in a simulation of GPS and Galileo geometries to generate VPLs for each time epoch and candidate smoothing process identified in Section 3.0. The results in Section 4.0 identify particular smoothing procedures and time constants that are optimal depending on the operational context and the ionospheric state. Section 5.0 describes the different considerations that apply under anomalous ionospheric conditions, and Section 6.0 summarizes the paper.

2.0 THE ROLE OF SMOOTHING

Rather than making use of instantaneous ("raw") pseudorange (or "code") measurements, both GBAS and LADGNSS apply a standard technique known as carrier smoothing to reduce the multipath and thermal noise errors in these measurements. This is a vital step because the errors in raw code measurements are at the level of several meters (1σ) and are too large to satisfy the missions that GBAS and LADGNSS are intended to support. Existing GBAS ground and airborne receivers perform single-frequency (SF) low-pass smoothing using the method shown in Section 3.1A below with matched (same at ground and airborne) smoothing time constants of 100 seconds (GAST A – GAST C) and 30 seconds (GAST D) [14]. However, with dual-frequency measurements, other options exist, as described in Sections 3.1B and C below.

While SF GBAS maintains matched ground and airborne smoothing time constants, this is not required, particularly for the divergence-free (DF) and ionosphere-free (or "iono-free," IF) alternatives described below, as they apply dual-frequency measurements to remove the ionospheric code-carrier divergence that causes increased residual errors for SF smoothing. In general, longer smoothing times are preferred for ground receiver measurements to better attenuate the higher and longer time correlation of multipath errors at fixed ground antennas, but airborne receivers can make use of shorter smoothing times due to lower multipath and shorter time correlations on a moving vehicle some distance above the ground. In addition, UAV attitude changes are more likely to briefly block signals, interrupt carrier phase tracking, and require smoothing filters to be restarted when compared to fixed (and hopefully well-sited) ground antennas. Shorter smoothing time constants allow restarted filters to re-converge more quickly, which is another motivation for keeping airborne smoothing times short compared to those on the ground. These and other practical considerations motivate the development of detailed DFDC LADGNSS measurement error models and simulation of VPLs in order to identify which combinations of smoothing techniques and ground and airborne time constants are optimal under different circumstances.

3.0 MEASUREMENT PROCESSING METHODS AND ERROR MODELS

3.1 Code-carrier smoothing filter models and output

As explained in Section 2.0, LADGNSS applies carrier smoothing of code (pseudorange) measurements at the reference station and users to attenuate correlated (multipath) and uncorrelated (thermal noise) errors. The smoothing process updates past noisy code measurements with current carrier phase measurements which are less noisy but ambiguous. For the DFDC LADGNSS system, three types of smoothing processes can be implemented: Single Frequency (SF), Divergence-Free (DF), and Ionosphere (iono)-Free (IF). These processes use the same low-pass filter arrangement of Figure 1, but the inputs (Ψ_k, Φ_k) are different.

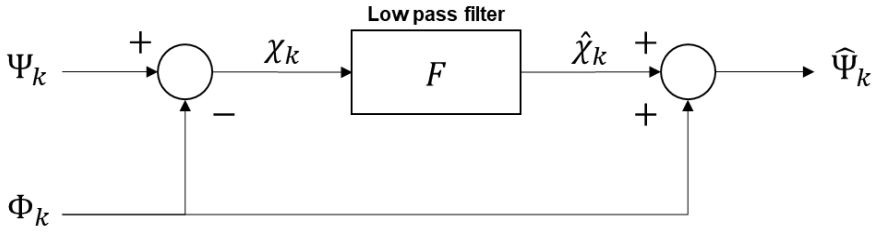

Figure 1: Generalized Carrier Smoothing Processing Technique

This section outlines the single frequency, divergence-free, and iono-free smoothing processes developed in previous work [1].

A. Single Frequency Smoothing and Output

In the single frequency smoothing process, code and carrier phase measurements from the same frequency are inputs to the filter:

$$\Psi_k = \rho_{x,k} = r + I_x + \eta_{\rho x} \tag{1}$$

$$\Phi_k = \psi_x = r - I_x + \lambda_x N_x + \eta_{\psi x} \tag{2}$$

where $\rho_{x,k}$ represents the frequency *x*, code measurement, $\psi_{x,k}$ is the frequency *x* carrier phase measurement at time epoch *k*, r is the geometric range plus errors common to both code and carrier phase, I_x is the ionospheric error, λ_x is the wavelength of frequency x, N_x is the carrier phase integer ambiguity, $\eta_{\rho x}$ is the thermal noise and multipath on code, and $\eta_{\psi x}$ is the thermal noise and multipath on carrier phase measurements.

For a given transfer function of the low-pass filter, $F(s)$, the Laplace transformed *x*-frequency-based smoothed code measurement, $\hat{\rho}_{x,k}$, is given by [1]:

$$\hat{\rho}_{x,SF}(\mathrm{s}) = r + (2F - 1)I_x(s) + F\eta_{\rho x} + (1 - F)\eta_{\psi x} \tag{3}$$

Eq. (3) shows that the additional error can be introduced by an ionospheric temporal gradient, $2FI_x(s)$, which induces what is known as Code-Carrier-Divergence (CCD). This error can be compensated by applying LADGNSS corrections in airborne receivers when both ground and airborne use an identical low-pass filter ($F_{gnd} = F_{air}$). The noise of the output is dominated by the SF smoothed thermal noise and multipath of frequency *x* code measurement, $F\eta_{\rho x}$.

B. Divergence-Free Smoothing and Output

The influence of ionospheric temporal gradients can be removed using a combination of carrier phase measurements from two different frequencies. The inputs of the *x*-frequency-based DF smoothing process are as follows [1]:

$$\begin{aligned} \Psi_k &= \rho_{x,k} = r + I_x + \eta_{\rho x} \\ \Phi_k &= \psi_{x,k} - \frac{2}{\alpha}\left(\psi_{x,k} - \psi_{y,k}\right) = r + I_x + N_{xy,k} + \eta_{\psi xy} + \frac{2}{\alpha}\left(IFB + \tau_{gd}\right) \end{aligned} \tag{4}$$

where $\psi_{y,k}$ denotes the frequency *y* carrier phase measurement at epoch *k*, $N_{xy,k}$ is the linear combination of the two frequencies' integer ambiguities, $\eta_{\psi xy}$ is the linear combination of two frequencies' carrier multipath and thermal noise, IFB is the inter-frequency bias of the receiver, which is caused by hardware differences between frequencies *x* and *y*, τ_{gd} is the inter-frequency bias of the signal transmitter, and α is a constant that equals $\left(1 - \frac{f_x^2}{f_y^2}\right)$ based on the first-order ionospheric refraction model [2] .

The output of the *x*-frequency-based DF smoothing process is expressed by the following equation with the transfer function of the low-pass filter, F [1]:

$$\hat{\rho}_{x,DF}(\mathrm{s}) = \mathrm{r} + I_x(s) + F\eta_{\rho x} + (1 - F)\eta_{\psi xy} \tag{5}$$

Although there is no ionospheric temporal gradient induced error (to first order), the DF smoothed code measurement still suffers from ionospheric error, $I_x(s)$. In other words, the difference between ground and airborne ionospheric error at a given epoch is a potential threat when anomalous ionospheric gradients are present. The noise of DF smoothed code measurement is dominated by the smoothed thermal noise and multipath of the frequency *x* code measurement, $F\eta_{\rho x}$, which is equivalent to the SF smoothed code measurement.

C. Iono-Free Smoothing and Output

The contribution of first order approximated ionospheric error can be removed using the combination of code and carrier phase measurements from two different frequencies. The inputs of the IF smoothing process are as follows [1]:

$$\Psi_k = \rho_{x,k} - \frac{1}{\alpha}\left(\rho_{x,k} - \rho_{y,k}\right) = r + \eta_{\rho xy} + \frac{1}{\alpha}(IFB + \tau_{gd}) \tag{6}$$

$$\Phi_k = \psi_{x,k} - \frac{1}{\alpha}\left(\psi_{x,k} - \psi_{y,k}\right) = \mathrm{r} + N_{xy,k} + \eta_{\psi xy} + \frac{1}{\alpha}\left(IFB + \tau_{gd}\right) \tag{7}$$

where $\rho_{y,k}$ is the frequency *y* code measurement, and $\eta_{\rho xy}$ is the linear combination of two frequencies' code multipath and thermal noise. The output of the IF smoothed process is expressed by Eq. (8) [1]:

$$\hat{\rho}_{IF}(\mathrm{s}) = \mathrm{r} + F\eta_{\rho xy} + (1-F)\eta_{\psi xy} + \frac{1}{\alpha}\left(IFB + \tau_{gd}\right) \tag{8}$$

which is significantly noisier than the outputs of the SF and DF processes described earlier. Assuming that the code measurements are statistically independent in time, measurements from different frequency are uncorrelated, and the contribution of carrier phase noise is negligible, the standard deviation of IF smoothed code measurement with a single-pole low-pass filter can be approximated as the following equation [1].

$$\sigma_{\rho xy,IF} \approx \sqrt{\frac{T}{2\tau}}\sqrt{\left(1-\frac{1}{\alpha}\right)^2 \sigma_{\rho x}^2 + \frac{1}{\alpha^2}\sigma_{\rho y}^2} \tag{9}$$

where T is GNSS measurement sampling time, $\sigma_{\rho x}$ is the standard deviation of frequency *x* code multipath and thermal noise, and $\sigma_{\rho y}$ is the standard deviation of frequency *y* code multipath and thermal noise.

The inter-frequency bias of the receiver (IFB) in the output of IF smoothed code measurement can be captured through receiver clock estimation by generating corrections for each constellation separately, and the inter-frequency bias of the transmitter (τ_{gd}) is also removed by applying these corrections.

3.2 Error models

To determine the optimal smoothing approach for the DFDC LADGNSS system, we compare simulated Vertical Protection Levels (VPLs) for each candidate which has different smoothing processes, ground and airborne smoothing time constants, and signal frequency. The VPLs are calculated using Eqs. (10) and (11) [3]:

$$VPL_{H0} = K_{ffmd}\sqrt{\sum_{i=1}^{N} S_{vert,i}^2 \cdot \sigma_i^2} \tag{10}$$

$$VPL_{eph} = \max_k\left(VPL_{eph,k}\right) \tag{11}$$

$$VPL_{eph,k} = \left|S_{vert,k}\right| x_{air} P_k + K_{md}\sqrt{\sum_{i=1}^{N} S_{vert,i}^2 \cdot \sigma_i^2} \tag{12}$$

where VPL_{H0} is the VPL under the fault-free hypothesis, K_{ffmd} is the multiplier to meet the allocated integrity risk requirement, $S_{vert,i}$ is the element of the weighted least square estimator projecting the i^{th} measurement into vertical position, σ_i is the standard deviation of a zero-mean Gaussian distribution bounding all range errors of the i^{th} corrected code measurement in the tails, $VPL_{eph,k}$ is the VPL under the k^{th} satellite ephemeris fault, x_{air} is the distance between reference station and user receiver, P_k is the ephemeris error decorrelation parameter for the k^{th} satellite ($P_k = 0.00018$ is used in this study, [4]), and K_{md} is the multiplier to satisfy the allocated missed detection probability of an ephemeris fault. The final VPL applied by the user is the maximum between VPL_{H0} and VPL_{eph}.

The standard deviation of the i^{th} corrected code measurement is decomposed as shown in Eq. (13) [3]:

$$\sigma_i^2 = \sigma_{gnd,i}^2 + \sigma_{air,i}^2 + \sigma_{iono,i}^2 + \sigma_{trop,i}^2 \tag{13}$$

where $\sigma_{gnd,i}$ denotes the standard deviation of the ground error contribution, $\sigma_{air,i}$ is the standard deviation of the airborne multipath and thermal noise, $\sigma_{iono,i}$ is the standard deviation of the ionospheric de-correlation and $\sigma_{trop,i}$ is the standard deviation of the tropospheric decorrelation for i^{th} satellite.

A. Ground Error Model, σ_{gnd}

The 1σ ground error model for the i^{th} satellite is decomposed as shown in Eqs. (14) and (15), assuming statistical independence of errors among reference receivers [5]:

$$\sigma_{gnd,i}^2 = \frac{\sigma_{pr\_gnd,i}^2}{M} + \sigma_{SIS}^2 \tag{14}$$

$$\sigma_{pr\_gnd,i}^2 = \sigma_{mp}^2(\theta_i) + \sigma_n^2(\theta_i) \tag{15}$$

where $\sigma_{mp}(\theta_i)$ denotes the standard deviation of ground multipath error, $\sigma_n(\theta_i)$ is the standard deviation of ground thermal noise, θ_i is the elevation angle of i^{th} satellite, and σ_{SIS} is the standard deviation of Signal-In-Space (SIS) error [5].

For GBAS, standard ground multipath and thermal noise error models are in [5] for GPS L1 with a 100-second ground smoothing time constant. However, in LADGNSS, reference receiver antennas are likely not spaced far enough apart to provide decorrelated errors, and a different smoothing procedure (e.g., SF or DF or IF with a different smoothing time or signal frequency) is likely to be applied. Under these conditions, the existing error models are no longer sufficient. To remove this limitation, a modified and more general ground error model is proposed. This ground error model is expressed by the following equation with a constant correlation coefficient (ρ) between reference receivers:

$$\sigma_{gnd,i}^2 = \xi^2 \left({\sigma_{mp}^*}^2(\rho, \theta_i) + {\sigma_n^*}^2(\theta_i) \right) + \sigma_{SIS}^2 \tag{16}$$

where ξ is the ratio between the 100s, SF smoothed measurement error standard deviation and the actual procedure applied (SF or DF or IF smoothed measurement error standard deviation with a different smoothing time constant), $\sigma_{mp}^*(\rho, \theta_i)$ is the modified standard deviation of ground multipath with a constant correlation coefficient between reference receivers, and $\sigma_n^*(\theta_i)$ is the modified standard deviation of ground thermal noise.

The difference of standard deviations between SF and DF smoothed code multipath and thermal noise are negligible because both cases are dominated by the same noise term from the input code measurement (shown in Section 3.1). Thus, ξ can be defined as the ratio of the standard deviation of 100-second SF and τ-second SF or IF smoothed code multipath and thermal noise (where the SF ratio for a given τ also incorporates the "DF" case). $\xi(\tau)$ using a different smoothing time can be expressed as the following equation using the First Order Gauss Markov (FOGM) model for correlated code measurement errors [15]:

$$\xi(\tau) = \sqrt{\frac{\left(\left(\frac{T}{\tau}\right)^2 \sum_{i=1}^{\tau/T} \left(1 - \frac{T}{\tau}\right)^{2(i-1)} + 2\left(\frac{T}{\tau}\right)^2 \sum_{i=1}^{\tau/T} \sum_{\substack{j=1 \\ j \neq i}}^{\tau/T} \left(1 - \frac{T}{\tau}\right)^{i+j-2} exp\left(-\frac{|i-j|T}{\tau_{corr}}\right) \right)}{\left(\left(\frac{T}{100}\right)^2 \sum_{i=1}^{100/T} \left(1 - \frac{T}{100}\right)^{2(i-1)} + 2\left(\frac{T}{100}\right)^2 \sum_{i=1}^{100/T} \sum_{\substack{j=1 \\ j \neq i}}^{100/T} \left(1 - \frac{T}{100}\right)^{i+j-2} exp\left(-\frac{|i-j|T}{\tau_{corr}}\right) \right)}} \tag{17}$$

where T is the GNSS measurement sampling time, τ is the smoothing time constant, and τ_{corr} is the correlation time constant of the FOGM. Values of $\xi(\tau)$ for 60, 30, and 15-second smoothing time constants with the 30-second correlation time constant are shown in Table 1. The 30-second correlation time constant was determined based on the averaged autocorrelation coefficient of GPS L1 code measurements collected at KAIST in Daejeon, Korea. The derivation of Eq. (17) is presented in Appendix A.

Table 1: Standard Deviation Ratio between 100s and Different Smoothing Time Constants

	$\tau = 60$s	$\tau = 30$s	$\tau = 15$s
$\xi(\tau)$	1.1486	1.3026	1.3997

For IF smoothed code measurements with time constant τ, the additional constant based on Eq. (9) is multiplied by $\xi(\tau)$ (in this study, a constant IF multiplier of 2.4267 is used for L1/E1 and L5/E5a measurements [6]).

If the ground uses a different frequency code measurement based smoothing process (e.g. GPS L5 based SF, Galileo E5a based SF, etc.), the multipath and thermal noise differences have to be addressed. To do this, we multiply the standard deviations of the two frequencies' thermal noise and multipath errors by a constant ratio. The ratios for GPS L1/L5 and Galileo E1/E5a in Table 2 are used in this study (note that these values are more conservative than those suggested in [6]).

Table 2: Standard Deviation Ratio between Measurements from Two Different Frequencies

	Galileo E1	Galileo E5a
GPS L1	1	1.43 (= 1/0.7)
GPS L5	0.7	1

${\sigma_{mp}^*}^2(\rho, \theta_i)$ is expressed by the following equation, assuming a correlation coefficient between ground receivers of ρ:

$$ {\sigma_{mp}^*}^2(\rho, \theta_i) = \frac{\big(1 + 2\rho(M-1)\big)}{MN^2}\left(\sum_{\substack{j=1 \\ j\neq i}}^{N} GAD_{mp}\big(\theta_j\big)^2 + \frac{(N-1)^2}{MN^2} GAD_{mp}(\theta_i)^2\right) \tag{18} $$

where $GAD_{mp}\big(\theta_j\big)$ is the GAD multipath model for the j^{th} satellite, M is the number of ground receivers, N is the number of GNSS measurements, and θ_j is the elevation angle of the j^{th} satellite.

${\sigma_n^*}^2(\theta_i)$ is expressed by the following equation assuming statistical independence of thermal noise among receivers:

$$ {\sigma_n^*}^2(\theta_i) = \frac{1}{MN^2}\sum_{\substack{j=1 \\ j\neq i}}^{N} GAD_n(\theta_j)^2 + \frac{(N-1)^2}{(MN)^2} GAD_n(\theta_i)^2 \tag{19} $$

where $GAD_n(\theta_j)$ is the GAD thermal noise model for the j^{th} satellite. The SIS error models (including those for GAD) and corresponding standard deviations are given in [3], and GAD-C numbers are used in the study. σ_{SIS} consists of the root-sum-square of the standard deviation of each error source except for ground to airborne multipath, which can be significant for UAVs flying close to the ground but can also be attenuated through the airborne smoothing process. Eqs. (18) and (19) are derived in Appendix B.

B. Airborne Error Model, σ_{air}

The 1σ airborne error model for i^{th} satellite is decomposed as shown in Eq. (20) [3]:

$$ \sigma_{air,i}^2 = \sigma_{mp,air}^2(\theta_i) + \sigma_{n,air}^2(\theta_i) \tag{20} $$

where $\sigma_{mp,air}(\theta_i)$ is the standard deviation of airborne multipath error, and $\sigma_{n,air}(\theta_i)$ is the standard deviation of airborne thermal noise for the i^{th} satellite (these are defined in [3]).

The modified airborne error model for a different smoothing time constant and smoothing processes is expressed as

$$ \sigma_{air,i}^2 = \xi(\tau_{air})^2\big(\sigma_{mp,air}^2(\theta_i) + \sigma_{n,air}^2(\theta_i)\big) \tag{21} $$

where τ_{air} is the airborne smoothing time constant. The considerations for different frequencies, smoothing processes, and smoothing time constants are identical to those for the ground error model.

C. Ionospheric Error Model, σ_{iono}

The ionospheric error model is defined differently depending on the smoothing process applied [7]:

$$\sigma_{iono,SF} = F_{pp} \times \sigma_{vig} \times (x_{air} + 2\tau_{air} v_{air}) \tag{22}$$

$$\sigma_{iono,DF} = F_{pp} \times \sigma_{vig} \times x_{air} \tag{23}$$

$$\sigma_{iono,IF} = 0 \tag{24}$$

where F_{pp} represents the vertical-to-slant ionospheric thin-shell-model obliquity factor [3], σ_{vig} is the standard deviation of a normal distribution associated with the residual ionospheric uncertainty due to spatial gradients (e.g., between reference station and airborne user) in the vertical domain and is expressed in terms of $\mathrm{mm/km}$, x_{air} is the distance from user to reference station as before, and v_{air} is the 2-D horizontal airborne user velocity. Note that Eq. (22) can only be used when both ground and airborne use the identical smoothing time constant because Eq. (22) does not consider the Code-Carrier-Divergence (CCD) induced by the ionospheric temporal gradient. Thus, the contribution of the ionospheric temporal gradient must be addressed for a general SF smoothing process. The modified ionospheric error model, $\sigma^*_{iono,SF}$,for the SF smoothed code measurement is expressed in Eq (25):

$$\sigma^*_{iono,SF}{}^2 = \sigma^2_{iono,SG} + \sigma^2_{iono,TG} \tag{25}$$

where $\sigma_{iono,SG}$ denotes the contribution of ionospheric spatial gradients, and $\sigma_{iono,TG}$ is the contribution of ionospheric temporal gradients. Both terms with τ_{gnd} ground time constant and τ_{air} airborne time constant are expressed as follows:

$$\sigma_{iono,SG} = F_{pp} \times \sigma_{vig} \times (x_{air} + 2\tau_{air} v_{air}) \tag{26}$$

$$\sigma_{iono,TG} = 2 \times \sigma_{iono\ gradient\ rate} \times |\tau_{gnd} - \tau_{air}| \tag{27}$$

where $\sigma_{iono\ gradient\ rate}$ is the standard deviation of a normal distribution associated with the residual ionospheric uncertainty due to temporal variation of ionospheric delay at a fixed location and is expressed in terms of $\mathrm{m/s}$. These ionospheric error models also depend on the signal frequency, which is addressed through the first order ionospheric refraction model. In particular, ionospheric error standard deviations for L5/E5a measurement based smoothing processes are multiplied by a factor of 1.79 over the same standard deviations for L1/E1 due to the fact that L5/E5a is at a lower frequency than L1/E1 and thus suffers more ionospheric delay and delay variability.

D. Tropospheric Error Model, σ_{trop}

The tropospheric error model in [5] considers the contribution of nominal tropospheric decorrelation only. The non-nominal tropospheric decorrelation addressed in [8] has the same x_{air} dependency as ionospheric spatial decorrelation, thus GBAS uses an increased σ_{vig} by combining non-nominal tropospheric decorrelation and ionospheric spatial decorrelation instead of using two separate sigma values. However, if the IF smoothing process is considered, the residual ionospheric uncertainty is (approximately) zero as shown in Eq. (24), and consequently non-nominal tropospheric decorrelation cannot be addressed. Thus, it is necessary to consider these two terms separately. A modified tropospheric error model (σ^*_{trop}) is expressed in Eq. (28), assuming statistical independence between nominal and non-nominal tropospheric errors.

$$\sigma^*_{trop}{}^2 = \sigma^2_{tropo,nominal} + \sigma^2_{tropo,non-nominal} \tag{28}$$

Each term of Eq. (28) is defined as [8]:

$$\sigma_{tropo,nominal} = \sigma_N h_0 \frac{10^{-6}}{\sqrt{0.002 + sin^2\theta}} \left(1 - e^{\frac{\Delta h}{h_0}}\right) \tag{29}$$

$$\sigma_{tropo,non-nominal} = F_{pp} \times \sigma_{non-nominal-tropo} \times x_{air} \tag{30}$$

where σ_N is the tropospheric refractivity index uncertainty, h_0 is the tropospheric scale height, Δh is the height of the users above the LADGNSS reference station, and $\sigma_{non-nominal-tropo}$ is the standard deviation that covers anomalous tropospheric threats. The tropospheric error does not change depending on the smoothing mode, and thus the same model is used for all candidates.

4.0 SIMULATION PROCEDURE AND RESULTS

4.1 Simulation Conditions

The simulation is conducted to compare the VPL of the operation mode candidates. The primary operation mode candidates of the DFDC LADGNSS system are in Table 3. The right-hand side of this table shows the five combinations of ground and airborne smoothing times that are considered.

Table 3: Candidate Smoothing Modes

Smoothing Process	Smoothing Time Constant
L1/E1 based Single Frequency Smoothing	$(\tau_{gnd}, \tau_{air}) \in \{(15s, 15s), (30s, 15s), (30s, 30s), (60s, 30s), (60s, 60s)\}$
L1/E1 based Divergence-Free Smoothing	
L5/E5a based Single Frequency Smoothing	
L5/E5a based Divergence-Free Smoothing	
Ionosphere-Free Smoothing	

In the simulation, the DFDC LADGNSS measurements are based on the 27-satellite "expandable" GPS constellation given in Section 3.2 of [12] transmitting L1 and L5 and a 27-satellite Galileo constellation transmitting E1 and E5a. A 10° elevation mask angle for satellite visibility is used for both constellations. Other parameters used in this simulation are shown in Table 4.

Table 4: Key Simulation Parameters

Parameter	Value [Unit]
M	3
x_{air}	5 $[km]$
v_{air}	15 $[m/s]$
ρ	0.1
σ_{vig}	4 $[mm/km]$ [9]
$\sigma_{iono\ gradient\ rate}$	0.004 $[m/s]$
σ_N	23 [8]
h_0	15,730 $[m]$ [8]
$\sigma_{tropo,non-nominal}$	5 $[mm/km]$ [8]

Twice the ionospheric delay temporal rate of change parameter for mid-latitudes in [3] is used as $\sigma_{iono\ gradient\ rate}$ in Table 4.

Simulations are conducted for two operational scenarios. The first scenario represents LADGNSS operations at fixed reference sites more similar to GBAS. For this scenario, GBAS error models GAD-B for ground, AAD-A for airborne error model, and a ground error correlation coefficient of 0.1 are used. The second scenario represents a portable, low-cost reference station that is designed to be re-sited frequently and re-surveyed quickly within a relatively small footprint. For this scenario, the less-accurate GAD-A for ground error is used along with AAD-A for airborne error and a ground error correlation coefficient of 0.6, representing ground receiver antennas sited within 10 – 20 meters of each other. Both sets of simulations are conducted over one day of satellite geometries with 600 seconds between time epochs.

4.2 Simulation Results

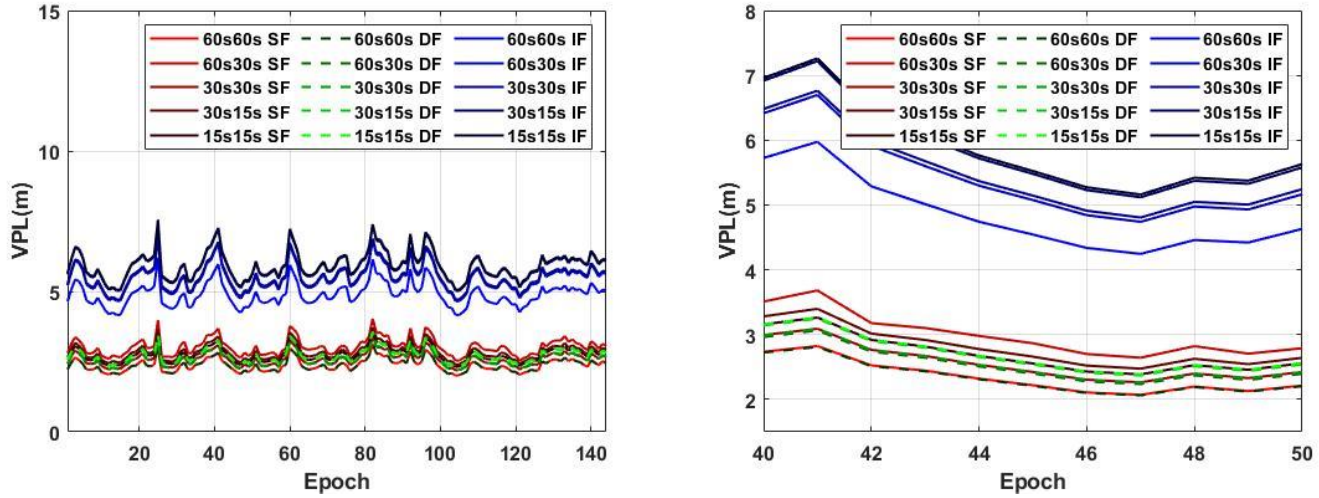

Figure 2: VPLs for L1/E1-based smoothing processes for the first scenario: full day (Left) and zoomed-in version (Right). The blue solid lines are VPLs from the IF smoothing process, the green dotted lines are VPLs from the DF smoothing process, and the red solid lines are VPLs from the SF smoothing process. In the legend, smoothing time constants are in the order of (ground, airborne) before the smoothing process type.

Figure 2 shows the VPLs generated for the first scenario by the L1/E1-based smoothing processes. For a fixed smoothing time constant, the largest VPL is obtained using the IF smoothing process (blue line) because the IF smoothed code measurement is significantly noisier than the others. VPLs for the IF smoothing process are also the most sensitive to changes in the smoothing time constants. VPLs with IF and DF smoothing processes decrease as smoothing times increase. This holds even for mismatched cases, in which the ground and airborne time smoothing constants are different. However, for SF smoothing, mismatched cases with longer smoothing times (e.g., 60s / 30s) may have larger VPLs than those of matched cases with shorter smoothing times (e.g., 30s / 30s) due to the contribution of temporal ionospheric gradients. These results confirm that there are no significant differences between the VPLs of the SF and DF smoothing processes with identical (matched) time constants for the ground and airborne because the divergence induced by airborne motion is insignificant due to the slow airborne speed (v_{air}) of 15 m/s assumed for UAVs.

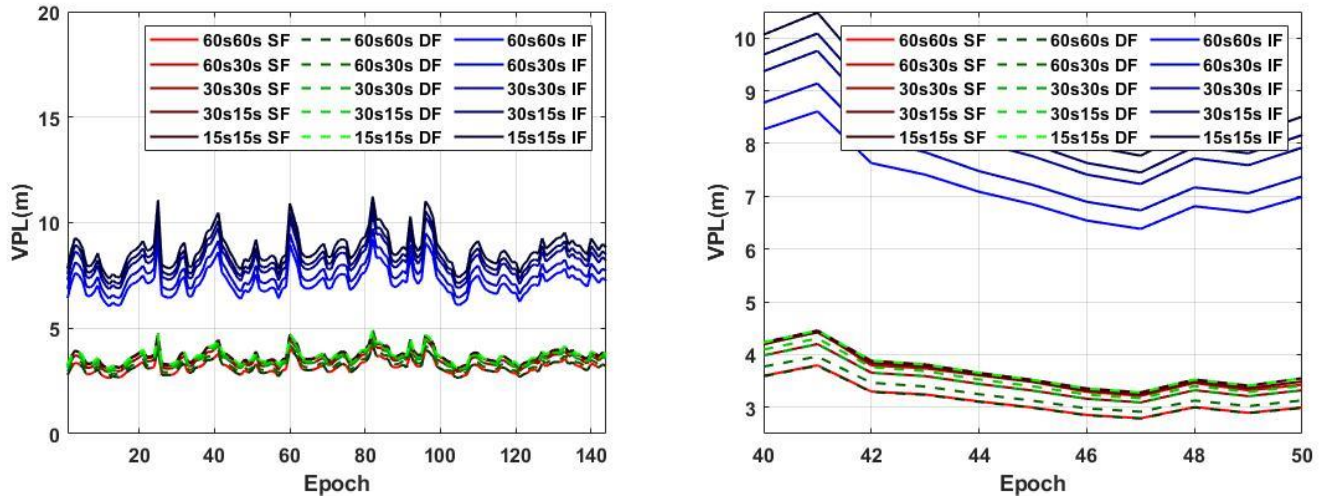

Figure 3: VPLs for L1/E1-based smoothing processes for the second scenario: full day (Left) and zoomed-in version (Right). The blue solid lines are VPLs from the IF smoothing process, the green dotted lines are VPLs from the DF smoothing process, and the red solid lines are VPLs from the SF smoothing process. In the legend, smoothing time constants are in the order of (ground, airborne) before the smoothing process type.

Figure 3 shows the VPLs generated for the second scenario by the same L1/E1-based smoothing processes. All VPLs in Figure 3 increase from what is shown in Figure 2 due to increased ground error contribution, and the degree of increase depends on the smoothing process. The smoothing time mismatched cases for the SF smoothing process are not worse than any matched cases for the DF or SF smoothing processes because, for this scenario, the (smoothing-attenuated) ground multipath and receiver noise error is much larger than the contribution of divergence induced by temporal ionospheric gradients.

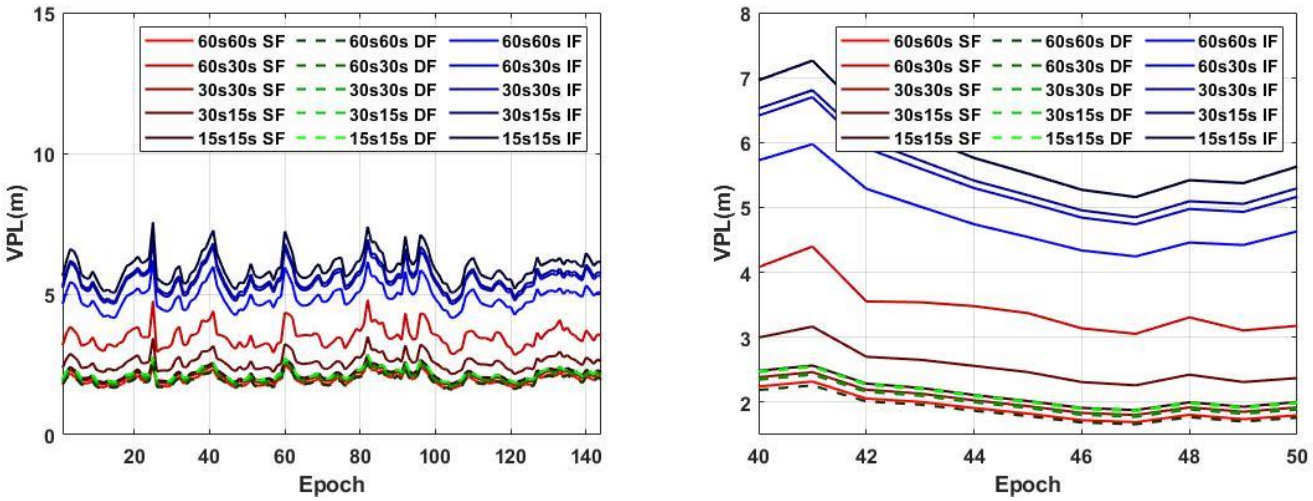

Figure 4: VPLs for L5/E5a-based smoothing processes for the first scenario: full day (Left) and zoomed-in version (Right). The blue solid lines are VPLs from the IF smoothing process, the green dotted lines are VPLs from the DF smoothing process, and the red solid lines are VPLs from the SF smoothing process. In the legend, smoothing time constants are in the order of (ground, airborne) before the smoothing process type.

Figure 4 returns to the first operational scenario but shows the VPLs generated by smoothing processes that use L5/E5a as the base (first) frequency. As noted above, ionospheric error contribution increases by 1.79 times L1/E1 for L5/E5a based smoothing. Therefore, the differences between VPLs with IF smoothing and those with DF and SF decrease, while the differences between VPLs with SF and DF for different (mismatched) ground and airborne smoothing times increase. For the time-constant-matched cases, VPLs decrease somewhat from those in Figure 2 due to the lower multipath and thermal noise of L5/E5a code measurements.

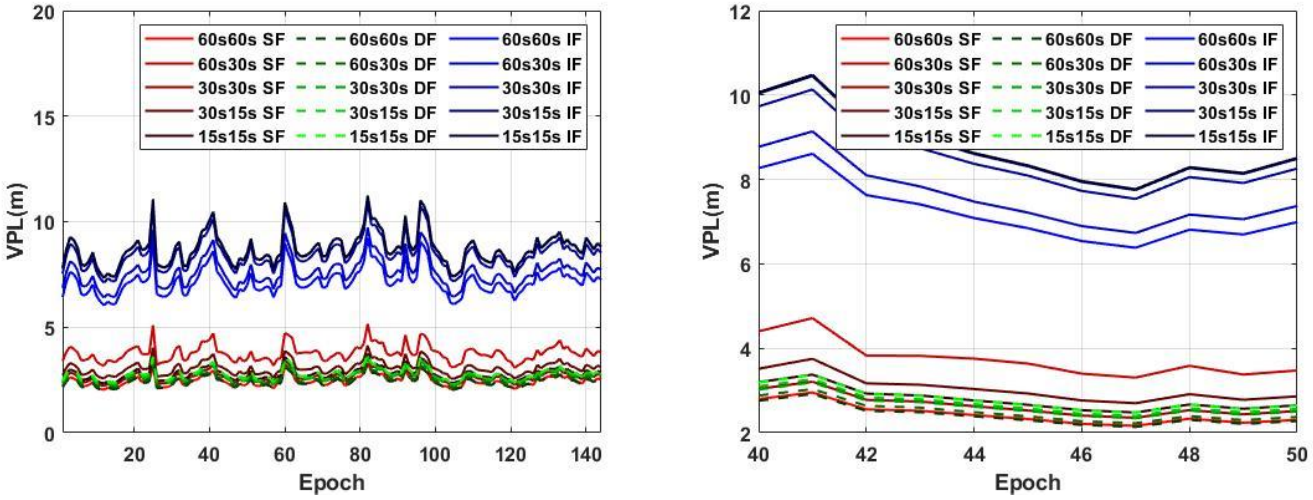

Figure 5: VPLs for L5/E5a-based smoothing processes with the first scenario: full day (Left) and zoomed-in version (Right). The blue solid lines are VPLs from the IF smoothing process, the green dotted lines are VPLs from the DF smoothing process, and the red solid lines are VPLs from the SF smoothing process. In the legend, smoothing time constants are in the order of (ground, airborne) before the smoothing process type.

Figure 5 shows the VPLs generated for the second scenario by the L5/E5a-based smoothing processes. These VPLs are more sensitive to changes in ground smoothing time than the first scenario due to the increased ground error contribution (GAD-A) of the second scenario. However, VPLs for the SF smoothing processes with different ground and airborne smoothing times are larger than any VPLs for SF with identical ground and airborne smoothing times or DF because the contribution of increased ionospheric error for L5/E5a is still dominant.

4.3 Sensitivity Analysis

Many parameters affect the performance of LADGNSS under nominal error conditions. Thus, it is important to analyze the sensitivity of the results to changes in these parameters when determining the optimal smoothing procedure. In this study, sensitivity analysis is conducted for the parameters that are inputs to the ionospheric error model, which is typically the largest error in LADGNSS: distance from user to LADGNSS reference station (x_{air}) and ionospheric spatial gradient (σ_{vig}) which varies with latitude.

A. Distance to LADGNSS Reference Stations

The distance from an airborne user to the centroid of the LADGNSS reference station antennas (which are typically not far apart) affects the component of the differential ionospheric range error that is insensitive to the airborne smoothing time constant. Therefore, simulations are conducted for the 30-second ground and 30-second airborne smoothing time case only. The simulation parameters are identical to those in Section 4.1 and Table 4 except that the distance between user and LADGNSS reference station is varied between $0 \leq x_{air} \leq 40$ km.

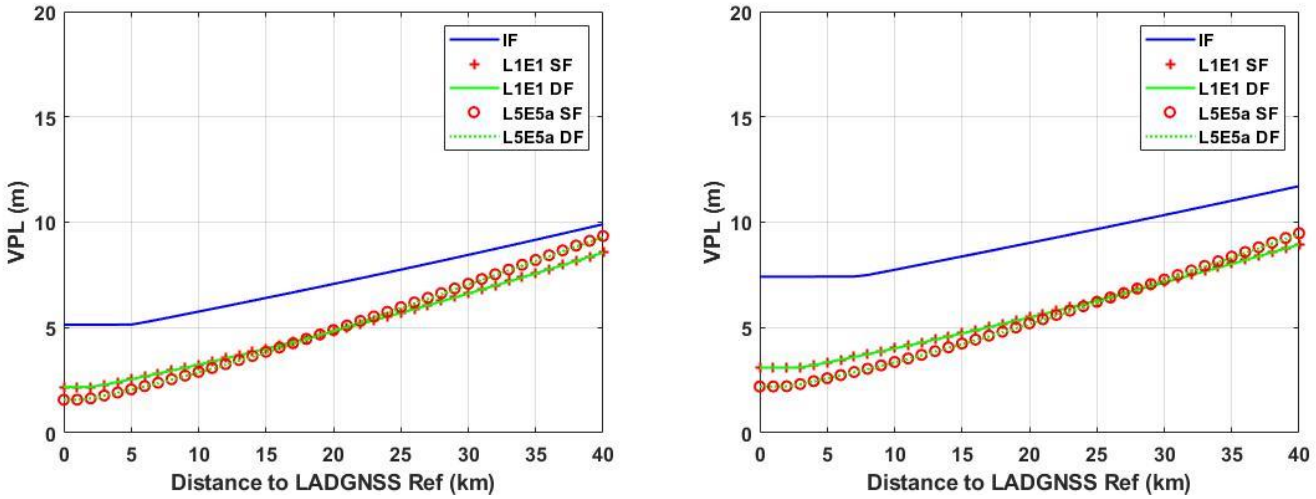

Figure 6: VPLs for the first scenario (Left) and the second scenario (Right) at one specific epoch (January 1, 2009, 00:00:00) as a function of the distance between airborne user and LADGNSS reference station. The red plus is the L1/E1-based SF smoothing process, the red circle is the L5/E5a-based SF smoothing process, the green solid line is the L1/E1-based DF smoothing process, the green dotted line is the L5/E5a-based DF smoothing process, and the blue solid line is the IF smoothing process.

Figure 6 shows VPLs at the first time epoch (January 1, 2009, 00:00:00) as a function of distance to LADGNSS reference station for the first and second operational scenarios. The general trend in Figure 6 is that the VPLs of the IF smoothing process increase linearly beyond the point where VPL_{eph} becomes larger than VPL_{H0} due to the increasing maximum undetected ephemeris error as x_{air} increases (see Eq. (12)). VPLs for the DF and SF smoothing processes show more rapid growth those for IF due to increasing differential ionospheric error as x_{air} increases. As a result, "transition points" exist where the VPLs with L5/E5a based SF and DF smoothing processes become larger than the VPLs with L1/E1 based SF and DF. This occurs where the larger ionospheric errors of L5/E5a begin to exceed the gap generated by the lower multipath and noise contribution of L5/E5a compared to L1/E1. These transition points are important because the optimal smoothing solution can vary depending on the user distance within a given LADGNSS coverage region. The closest transition points to the LADGNSS reference station based on one day of simulations are located at about 15 km for the first scenario and 20 km for the second scenario, respectively. The transition point of the first scenario is closer to the LADGNSS reference station than the second scenario because the contribution of large ground errors (GAD-A with

a ground error correlation coefficient of 0.6) in the second scenario creates a larger difference between L5/E5a-based and L1/E1-based VPLs.

The transition points where VPLs with SF or DF smoothing processes become larger than the VPL with IF smoothing process can also be defined. However, for mid-latitudes, those points are located outside the LADGNSS coverage volume with a radius of 40 km proposed in [10]. As a result, the IF smoothing process is not a candidate under consideration during nominal conditions.

B. Distance to LADGNSS Reference Stations for Equatorial Latitudes

The standard deviation of a normal distribution associated with residual ionospheric uncertainty due to ionospheric spatial gradients under nominal and active (but not rare) conditions (σ_{vig}) depends on latitude, as noted above. This sensitivity study is conducted for the 30s ground and 30s airborne smoothing time case but for equatorial regions near the magnetic equator here the ionosphere is much more active. The simulation parameters are identical to the previous subsection (including $0 \leq x_{air} \leq 40$ km) but with a much larger value of σ_{vig} = 13 mm/km (see [11]).

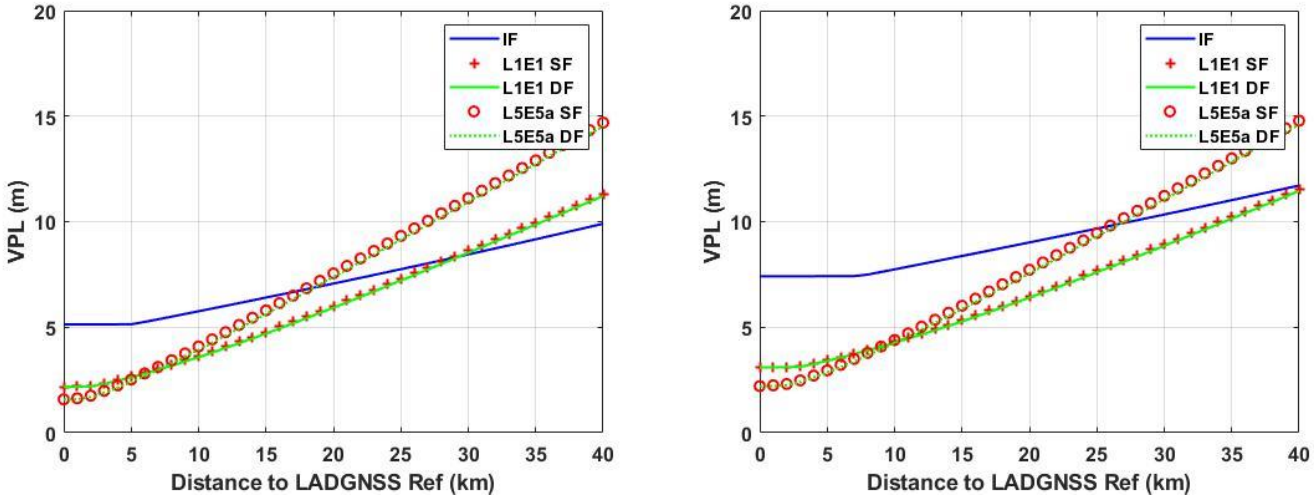

Figure 7: VPLs for the first scenario (Left) and the second scenario (Right) at the same epoch as Figure 7 as a function of the distance between airborne user and LADGNSS reference station. The red plus is the L1/E1-based SF smoothing process, the red circle is the L5/E5a-based SF smoothing process, the green solid line is the L1/E1-based DF smoothing process, the green dotted line is the L5/E5a-based DF smoothing process, and the blue solid line is the IF smoothing process. In these plots, a larger value of σ_{vig} = 13 mm/km is used to represent equatorial ionospheric conditions.

Figure 7 shows PLs as a function of distance from user to LADGNSS reference station in equatorial regions where the higher value of σ_{vig} applies. Compared to Figure 6 for mid-latitudes, VPLs for equatorial regions are more sensitive to changes in the distance from user to LADGNSS reference station due to the higher value of σ_{vig}, which is multiplied by x_{air} in Eq. (22). Therefore, the transition points defined previously are located closer to the LADGNSS reference station then in mid-latitudes. The closest transition points where the VPLs with L5/E5a based SF and DF smoothing processes become larger than the VPLs with L1/E1 based SF and DF based on one day of simulations are located at about 5 km for the first scenario and 10 km for the second scenario, respectively. The transition points where VPLs with SF or DF smoothing processes become larger than VPLs with IF are also located closer to the LADGNSS reference station. The closest transition points based on this simulation are shown in in Table 5.

Table 5: Transition Points for SF and DF vs. IF (larger σ_{vig})

	First Scenario	Second Scenario
Transition Point of L1/E1	27 km	20 km
Transition Point of L5/E5a	17 km	12 km

Thus, in equatorial regions, there are values of x_{air} where IF-based smoothing has the best performance for LADGNSS under nominal conditions, with the exception of the L1/E1-based smoothing process under the second scenario. Based on this and the knowledge that IF-based smoothing is more valuable under anomalous ionospheric conditions, IF-based smoothing remains a useful approach for LADGNSS to consider.

5.0 ANOMALOUS IONOSPHERIC CONSIDERATIONS

The results in Section 4.0 identify subsets of the possible smoothing procedures and time-constant choices that perform better (generate lower VPLs) for LADGNSS under nominal conditions as a function of parameters like the expected distance between users and the reference system (x_{air}) and the standard deviation that bounds nominal and active ionospheric spatial gradients (σ_{vig}). However, very large and difficult-to-bound errors caused by anomalous ionospheric spatial gradients have at least an equal impact on LADGNSS availability, particularly in equatorial regions where ionospheric anomalies are more common and more severe [16]. Mitigation of these anomalies by a DFDC LADGNSS borrows from GBAS and is mostly based on estimates of ionospheric delay magnitudes and rates of change for each satellite tracked by both ground and user receivers.

Under these conditions, the optimal smoothing procedures may be significantly different from those shown to be most desirable under nominal conditions in Section 4.0. For example, as mentioned above, IF-based smoothing becomes much more beneficial when the ionospheric delay difference between LADGNSS reference station and user becomes very large, as removing the delay almost entirely (in IF) is much better than only removing the delay difference over time (as in DF). In addition, while longer (matched) smoothing times are better for averaging code multipath errors under nominal conditions, they magnify the impact of large ionospheric gradients, as shown in Eq. (21).

We are currently studying the behavior of the candidate smoothing procedures described above under anomalous ionospheric conditions in order to resolve the trade-off between minimizing VPL under nominal vs. anomalous ionospheric conditions. A major complication of this analysis is the fact that, while worst-case ionospheric errors for GBAS occur when aircraft are approaching the GBAS reference station during precision approach operations [17], LADGNSS users will move in all directions relative to the reference station location, making it more complicated to identify the aircraft-to-ground geometries that cause the largest potential errors. Results from these studies will be published in a future paper.

6.0 SUMMARY

This paper examines several candidate smoothing procedures for a proposed dual-frequency, dual-constellation (DFDC) LADGNSS to support autonomous users such as airborne UAVs. New models of LADGNSS ground and airborne errors under nominal conditions are developed to address multipath errors that are statistically correlated over time and among multiple ground reference receivers. Using these models, detailed comparisons are made among the VPLs achieved by the candidate smoothing procedures and time constants. Depending on the operational context, including the local ionospheric conditions, the distances that UAVs operate from the LADGNSS ground system, and the quality of the ground equipment and siting environment, best-performing SF, DF, or IF processes and combinations of ground and airborne smoothing time constants are identified. Typically, under nominal conditions, longer (up to 60s) smoothing times that are the same for both ground and airborne measurements are preferred, and SF or DF smoothing is preferred to IF. Current work is examining how the optimal smoothing procedures change when anomalous ionospheric conditions and variable UAV flight paths relative to the LADGNSS ground system are considered.

APPENDIX A: DERIVATION OF MULTIPATH AND THERMAL NOISE CORRELATION IMPACT ACROSS TIME

This appendix derives Eq. (17), which represents the impact of multipath and thermal noise time correlation**.** $\xi(\tau)$ in Eq. (17) is defined as the ratio of the standard deviation of 100-second SF and τ-second SF smoothed code multipath and thermal noise.

$$\xi(\tau) = \frac{\sigma(\tau)}{\sigma(100s)} \tag{A1}$$

The standard deviation of τ second, SF smoothed code multipath and thermal noise, which is the numerator of Eq. (A1), can be calculated using the SF smoothing equation.

$$\hat{\eta}_{x,SF}(k) = \frac{T}{\tau}\eta_{\rho x}(k) + \frac{\tau - T}{\tau}\left[\hat{\eta}_{x,SF}(k-1) + \eta_{\psi x}(k) - \eta_{\psi x}(k-1)\right] \tag{A2}$$

where $\hat{\eta}_{x,SF}(k)$ is the frequency x-based SF smoothed code multipath and thermal noise with a τ-second smoothing time constant at the k^{th} epoch, $\eta_{\rho x}$ is the code multipath and thermal noise of frequency x, $\eta_{\psi x}(k)$ is the carrier phase multipath and thermal noise of frequency x, and T is the measurement sampling time. Eq. (A2) can be approximated as a function of code multipath and thermal noise as shown in Eq. (A3) while assuming the contribution of carrier phase noise is negligible.

$$\hat{\eta}_{x,SF}(k) \approx \left(\frac{T}{\tau}\right)\sum_{k=1}^{\tau/T}\left(1 - \frac{T}{\tau}\right)^{k-1}\eta_{\rho x}(k) \tag{A3}$$

Based on Eq. (A3), the variance of τ-second, SF smoothed code multipath and thermal noise can be calculated as follows.

$$\sigma_x^2(\tau) = E\left[\hat{\eta}_{x,SF}(k)\cdot\hat{\eta}_{x,SF}(k)\right] = E\left[\left(\left(\frac{T}{\tau}\right)\sum_{i=1}^{\tau/T}\left(1 - \frac{T}{\tau}\right)^{i-1}\eta_{\rho x}(i)\right)\cdot\left(\left(\frac{T}{\tau}\right)\sum_{j=1}^{\tau/T}\left(1 - \frac{T}{\tau}\right)^{j-1}\eta_{\rho x}(j)\right)\right] \tag{A4}$$

where E[·] is the expectation operator. It is assumed that the mean of code multipath and thermal noise is zero, i.e., $E\left[\eta_{\rho x}(i)\right] = 0$. The right-hand side of Eq. (A4) can be expended as follows.

$$\begin{aligned} &E\left[\left(\left(\frac{T}{\tau}\right)\sum_{i=1}^{\tau/T}\left(1 - \frac{T}{\tau}\right)^{i-1}\eta_{\rho x}(i)\right)\cdot\left(\left(\frac{T}{\tau}\right)\sum_{j=1}^{\tau/T}\left(1 - \frac{T}{\tau}\right)^{j-1}\eta_{\rho x}(j)\right)\right] \\ &\quad= \left(\frac{T}{\tau}\right)^2 E\left[\sum_{i=1}^{\tau/T}\left(1 - \frac{T}{\tau}\right)^{2(i-1)}\eta_{\rho x}^2(i) + 2\sum_{i=1}^{\tau/T}\sum_{\substack{j=1\\ j\neq i}}^{\tau/T}\left(1 - \frac{T}{\tau}\right)^{i+j-2}\eta_{\rho x}(i)\cdot\eta_{\rho x}(j)\right] \\ &\quad= \left(\frac{T}{\tau}\right)^2\sum_{i=1}^{\tau/T}\left(1 - \frac{T}{\tau}\right)^{2(i-1)}E\left[\eta_{\rho x}^2(i)\right] + 2\left(\frac{T}{\tau}\right)^2\sum_{i=1}^{\tau/T}\sum_{\substack{j=1\\ j\neq i}}^{\tau/T}\left(1 - \frac{T}{\tau}\right)^{i+j-2}E\left[\eta_{\rho x}(i)\cdot\eta_{\rho x}(j)\right] \end{aligned} \tag{A5}$$

This paper assumes that the code multipath and thermal noise follows a First Order Gauss-Markov (FOGM) model, i.e., $E\left[\eta_{\rho x}(i)\cdot\eta_{\rho x}(j)\right] = \sigma_{\rho x}^2\cdot exp\left(-\frac{|i-j|T}{\tau_{corr}}\right)$, where τ_{corr} indicates a correlation time constant and $\sigma_{\rho x}^2$ is a variance.
Substituting the FOGM model into Eq. (A5) yields:

$$\sigma_x^2(\tau) = \left(\frac{T}{\tau}\right)^2\sum_{i=1}^{\tau/T}\left(1 - \frac{T}{\tau}\right)^{2(i-1)}\sigma_{\rho x}^2 + 2\left(\frac{T}{\tau}\right)^2\sum_{i=1}^{\tau/T}\sum_{\substack{j=1\\ j\neq i}}^{\tau/T}\left(1 - \frac{T}{\tau}\right)^{i+j-2}\sigma_{\rho x}^2\cdot exp\left(-\frac{|i-j|T}{\tau_{corr}}\right) \tag{A6}$$

By using Eq. (A6), Eq. (A1) can be expressed as follows.

$$\xi(\tau) = \frac{\sigma(\tau)}{\sigma(100s)} = \sqrt{\frac{\left(\frac{T}{\tau}\right)^2 \sum_{i=1}^{\tau/T}\left(1-\frac{T}{\tau}\right)^{2(i-1)} + 2\left(\frac{T}{\tau}\right)^2 \sum_{i=1}^{\tau/T}\sum_{\substack{j=1 \\ j\neq i}}^{\tau/T}\left(1-\frac{T}{\tau}\right)^{i+j-2} exp\left(-\frac{|i-j|T}{\tau_{corr}}\right)}{\left(\frac{T}{100}\right)^2 \sum_{i=1}^{100/T}\left(1-\frac{T}{\tau}\right)^{2(i-1)} + 2\left(\frac{T}{100}\right)^2 \sum_{i=1}^{100/T}\sum_{\substack{j=1 \\ j\neq i}}^{100/T}\left(1-\frac{T}{100}\right)^{i+j-2} exp\left(-\frac{|i-j|T}{\tau_{corr}}\right)}} \tag{A7}$$

APPENDIX B: DERIVATION OF MULTIPATH CORRELATION IMPACT ACROSS RECEIVERS

The derivation of Eq. (18) and Eq. (19) is based on the ground reference receiver correction model in [3]. The ground correction model for satellite i, PRc^i, with M reference receivers and N satellites is as follows.

$$PRc^i = t^i + I^i + T^i + \varepsilon^i + \sum_{j=1}^{M}\Delta T_j + \frac{1}{M}\sum_{j=1}^{M}\eta_j^i - \frac{1}{NM}\sum_{j=1}^{M}\sum_{k=1}^{N}\eta_j^k \tag{B1}$$

where t^i is the clock bias of satellite i, I^i is the ionospheric error, T^i is the tropospheric error, ΔT_j is the residual error of the j^{th} reference receiver clock bias [3], and η_j^i is the error that is uncorrelated between the reference station and airborne for satellite i and receiver j. The ground contribution to error in the corrected code measurement is the only last two terms of Eq. (B1), and these terms can be expressed as shown in Eq. (B2).

$$\frac{1}{M}\sum_{j=1}^{M}\eta_j^k - \frac{1}{NM}\sum_{j=1}^{M}\sum_{k=1}^{N}\eta_j^k = \frac{1}{M}\sum_{j=1}^{M}\left(\eta_{j,multipath}^k + \eta_{j,thermal}^k\right) - \frac{1}{NM}\sum_{j=1}^{M}\sum_{k=1}^{N}\left(\eta_{j,multipath}^k + \eta_{j,thermal}^k\right) \tag{B2}$$

where $\eta_{j,multipath}^k$ indicates the ground multipath error for satellite k and receiver j and $\eta_{j,thermal}^k$ is the ground receiver thermal noise. The variance of Eq. (B2) is as follows.

$$\begin{aligned}\sigma_{gnd,i}^2 = \mathrm{E}\Bigg[&\left(\frac{1}{M}\sum_{j=1}^{M}\left(\eta_{j,multipath}^i + \eta_{j,thermal}^i\right) - \frac{1}{NM}\sum_{j=1}^{M}\sum_{k=1}^{N}\left(\eta_{j,multipath}^k + \eta_{j,thermal}^k\right)\right) \\ &\cdot\left(\frac{1}{M}\sum_{n=1}^{M}\left(\eta_{n,multipath}^i + \eta_{n,thermal}^i\right) - \frac{1}{NM}\sum_{n=1}^{M}\sum_{m=1}^{N}\left(\eta_{n,multipath}^m + \eta_{n,thermal}^m\right)\right)\Bigg]\end{aligned} \tag{B3}$$

The implicit assumption behind Eq. (B3) is that the mean of multipath and thermal noise is zero. The paper assumes that the multipath and thermal noise have the following correlation.

$$\mathrm{E}\left[\eta_{i,multipath}^n \cdot \eta_{j,multipath}^m\right] = \begin{cases} GAD_{mp,i}^2, & for\ i = j\ and\ n = m \\ \rho \cdot GAD_{mp,i} \cdot GAD_{mp,j}, & for\ i \neq j\ and\ n = m \\ 0, & for\ all\ other\ cases \end{cases} \tag{B4}$$

$$\mathrm{E}\left[\eta_{i,thermal}^n \cdot \eta_{j,thermal}^m\right] = \begin{cases} GAD_{n,i}^2, & for\ i = j\ and\ n = m \\ 0, & for\ all\ other\ cases \end{cases}$$

where $GAD_{mp,i}$ is the GAD multipath error model for satellite i, ρ is the correlation coefficient between multipath errors of ground reference receivers, and $GAD_{n,i}$ is the GAD thermal noise error model for satellite i. It is assumed that the correlation coefficient between any pair of multipath errors is the same. Based on Eq. (B4), the variance of the ground contribution can be expressed as follows.

$$\sigma_{gnd,i}^2 = \frac{\left(1+2\rho(M-1)\right)}{MN^2}\left(\sum_{\substack{j=1\\ j\neq i}}^{N} GAD_{mp,j}^2 + \frac{(N-1)^2}{MN^2} GAD_{mp,i}^2\right) + \frac{1}{MN^2}\sum_{\substack{j=1\\ j\neq i}}^{N} GAD_{n,j}^2 + \frac{(N-1)^2}{MN^2} GAD_{n,i}^2 \quad \text{(B5)}$$

Eq. (B5) is identical to the sum of Eq. (18) and Eq. (19).

ACKNOWLEDGMENTS

Gihun Nam and Noah Minchan Kim received support for this work from the MSIT (Ministry of Science, ICT), Korea, under the High-Potential Individuals Global Training Program (No. 2020-0-01531) supervised by the Institute for Information & Communications Technology Planning & Evaluation (IITP).

REFERENCES

1. Hwang, P. Y., McGraw, G. A., Bader, J. R. (1999). "Enhanced Differential GPS Carrier-Smoothed Code Processing Using Dual-Frequency Measurements," *Navigation, 46*(2), 127-137. https://doi.org/10.1002/j.2161-4296.1999.tb02401.x

2. Konno, H., "Dual-Frequency Smoothing for CAT III LAAS: Performance Assessment Considering Ionosphere Anomalies," *Proceedings of the 20th International Technical Meeting of the Satellite Division of The Institute of Navigation (ION GNSS 2007)*, Fort Worth, TX, September 2007, pp. 424-437. http://web.stanford.edu/group/scpnt/gpslab/pubs/papers/Konno_IONGNSS_2007.pdf

3. *Minimum Aviation System Performance Standards (MASPS) for the Local Area Augmentation System (LAAS)*, Washington, DC, RTCA DO-245A, December 2004. https://my.rtca.org/NC__Product?id=a1B36000001IcjtEAC

4. Park, Y. S., Pullen, S., Enge, P., "Enabling LAAS Airport Surface Movement: Mitigating the Anomalies Ionospheric Threat," *Proceedings of the 2010 IEEE/ION Position, Location, and Navigation Symposium*, Indian Wells, CA, May 2010, pp. 667-679. http://web.stanford.edu/group/scpnt/gpslab/pubs/papers/Park_IEEEIONPLANS_2010_SurfaceMovement.pdf

5. McGraw, G. A., Murphy, T., Brenner, M., Pullen, S., Van Dierendonck, A. J., "Development of the LAAS Accuracy Models," *Proceedings of the 13th International Technical Meeting of the Satellite Division of The Institute of Navigation (ION GPS 2000)*, Salt Lake City, UT, September 2000, pp. 1212-1223. https://www.ion.org/publications/abstract.cfm?articleID=1523

6. Circiu, M.-S., Felux, M., Thölert, S., Antreich, F., Vergara, M., Sgammini, M., Enneking, C., Pullen, S., "Evaluation of GPS L5 and Galileo E1 and E5a Performance for Future Multi Frequency and Multi Constellation GBAS," *Proceedings of the 2015 International Technical Meeting of The Institute of Navigation*, Dana Point, CA, January 2015, pp. 374-382. https://www.ion.org/publications/abstract.cfm?articleID=12636

7. Suzuki, K., Pullen, S., Enge, P., Ono, T., "Evaluation of Dual-Frequency GBAS Performance using Data from Public Receiver Networks," *Proceedings of the 23rd International Technical Meeting of the Satellite Division of The Institute of Navigation (ION GNSS 2010)*, Portland, OR, September 2010, pp. 2592-2602. http://web.stanford.edu/group/scpnt/gpslab/pubs/papers/Suzuki_IONGNSS_2010_EvaluationOfDualFreqGBAS_C5-2paperl.pdf

8. van Graas, F., Zhu, Z., "Tropospheric Delay Threats for the Ground Based Augmentation System," *Proceedings of the 2011 International Technical Meeting of The Institute of Navigation*, San Diego, CA, January 2011, pp. 959-964. https://www.ion.org/publications/abstract.cfm?articleID=9542

9. Lee, J., Pullen, S., Datta-Barua, S., Enge, P. (2007). Assessment of Ionosphere Spatial Decorrelation for Global Positioning System-Based Aircraft Landing Systems. *Journal of Aircraft, 44*(5), 1662-1669. https://doi.org/10.2514/1.28199

10. Kim, M., Lee, J., Kim, D., Lee, J., "Keynote: Design of Local Area DGNSS Architecture to Support Unmanned Aerial Vehicle Networks: Concept of Operations and Safety Requirements Validation," *Proceedings of the ION 2017 Pacific PNT Meeting*, Honolulu, Hawaii, May 2017, pp. 992-1001. https://doi.org/10.33012/2017.15091

11. Chang, H., Yoon, M., Pullen, S., Marini-Pereira, L., Lee, J., "Ionospheric spatial decorrelation assessment for GBAS daytime operations in Brazil," *NAVIGATION*. 2021; 68(2): 391– 404. https://doi.org/10.1002/navi.418

12. *Global Positioning System Standard Positioning Service Performance Standard (GPS SPS PS)*, Washington, DC, U.S. Department of Defense, 5th Edition, April 2020. https://www.gps.gov/technical/ps/2020-SPS-performance-standard.pdf

13. Kim, D., Lee, J., Kim, M., Lee, J., Pullen, S., "High-Integrity and Low-Cost Local-Area Differential GNSS Prototype for UAV Applications," *Proceedings of ION GNSS+ 2017*, Portland, OR, September 2017., pp. 2031-2054. https://doi.org/10.33012/2017.15110

14. *Minimum Operational Performance Standards for GPS Local Area Augmentation System Airborne Equipment*. Washington, DC, RTCA DO-253D. July 2017. https://my.rtca.org/NC__Product?id=a1B36000003Gl7ZEAS

15. Nahavandchi, H., Joodaki, G. (2010), "Correlation analysis of multipath effects in GPS-code and carrier phase observations," *Survey Review*, *42*(316), 193–206. https://doi.org/10.1179/003962610x12572516251808

16. Yoon, M., Lee, J., Pullen, S., Gillespie, J., Mathur, N., Cole, R., de Souza, J. R., Doherty, P., Pradipta, R. (2017), "Equatorial plasma Bubble Threat parameterization to Support GBAS operations in the Brazilian region," *Navigation*, *64*(3), 309–321. https://doi.org/10.1002/navi.203

17. Kim, D., Yoon, M., Pullen, S., Lee, J., "Closed-Form Analysis of Undetected Range Errors due to Ionospheric Impacts for GBAS Category I Operations," *NAVIGATION*. 2021; 68(3): 507-519. https://doi.org/10.1002/navi.442